Mechanical detwinning device for anisotropic resistivity measurements in samples requiring dismounting for particle irradiation

E. I. Timmons, M A Tanatar, Yong Liu, Kyuil Cho, T A Lograsso, M. Kończykowski, R. Prozorov

Mechanical detwinning device for anisotropic resistivity measurements in samples requiring dismounting for particle irradiation

E. I. Timmons,[1, 2, a)] M. A. Tanatar,[1, 2, b)] Yong Liu,[1, c)] Kyuil Cho,[1, d)] T. A. Lograsso,[1, 3, e)] M. Kończykowski,[4, f)] and R. Prozorov[1, 2, g)]

[1)]*Ames Laboratory, USDOE, Ames, Iowa 50011, USA*

[2)]*Department of Physics and Astronomy, Iowa State University, Ames, Iowa 50011, USA*

[3)]*Department of Material Science and Engineering, Iowa State University, Ames, Iowa 50011, USA*

[4)]*Laboratoire des Solides Irradiés, CEA/DRF/IRAMIS, Ecole Polytechnique, CNRS, Institut Polytechnique de Paris, F-91128 Palaiseau, France*

(Dated: 27 May 2020)

Uniaxial stress is used to detwin samples of orthorhombic iron based superconductors to study their intrinsic electronic anisotropy. Here we describe the development of a new detwinning setup enabling variable-load stress-detwinning with easy sample mounting/dismounting without the need to re-solder the contacts. It enables the systematic study of the anisotropy evolution as a function of an external parameter when the sample is modified between the measurements. In our case, the external parameter is the dose of 2.5 MeV electron irradiation at low temperature. We illustrate the approach by studying resistivity anisotropy in single crystals of $Ba_{1-x}K_xFe_2As_2$ at $x = 0.25$ where the much discussed unusual re-entrance of tetragonal C_4 phase, $C_4 \rightarrow C_2 \rightarrow C_4$, is observed on cooling. With the described technique we found a significant anisotropy increase in C_2 phase after electron irradiation with dose of 2.35 C/cm^2.

I. INTRODUCTION

In iron-based superconductors the nematic in-plane anisotropy of electrical resistivity in strain-detwinned samples strongly depends on sample residual resistivity[1,2]. The anisotropy changes sign between electron- and hole- doped iron based superconductors[3] and it was argued that the sign change may be linked with dramatically different residual resistivities on electron- and hole doped sides[4]. Indeed substitution on transition metal side in electron-doped $Ba(Fe_{1-x}Co_x)_2As_2$ gives notably higher disorder and residual resistivity as compared to hole-doped $Ba_{1-x}K_xFe_2As_2$ in which substitution is performed into electronically inactive Ba site.

Low-temperature sample irradiation with relativistic 2.5 MeV electrons provides a controlled way to introduce point defects[5], altering residual resistivity of the samples[6–8]. In hole doped $Ba_{1-x}K_xFe_2As_2$ irradiation with reasonable doses of several C/cm^2 was shown to bring residual resistivity to the level comparable to the electron-doped compositions[7]. Targeting experiments on electron irradiated samples to directly test the effect of controlled disorder on in-plane resistivity anisotropy, we realized that none of the approaches used for sample detwinning[9] are compatible with electron irradiation, which stimulated us to design a detwinning device described here.

[a)]Electronic mail: erikt@iastate.edu
[b)]Electronic mail: tanatar@ameslab.gov
[c)]Electronic mail: yongliu31@outlook.com
[d)]Electronic mail: kcho@ameslab.gov
[e)]Electronic mail: lograsso@ameslab.gov
[f)]Electronic mail: marcin.konczykowski@polytechnique.edu
[g)]Electronic mail: prozorov@ameslab.gov

II. DESIGN CONSIDERATIONS

In the low-temperature electron irradiation facility at Laboratoire des Solides Irradiés (LSI)[10], a sample is immersed into liquid hydrogen at approximately 20 K, providing efficient sample cooling during irradiation to prevent defects from self-annealing. The liquid hydrogen surrounding sample is heated by electron beam both indirectly by heating the sample and the sample holder, and directly by heating the liquid itself. Thus, the cryogenic path of electron beam (thickness of sample space) should be kept at a minimum. In fact the sample space is limited to 5 mm diameter and 2 mm in thickness. In addition, the machine time for these experiments is available for a short period and with a big interval (typically twice a year), so that sample stress application needs to be separated from the irradiation process.

III. DESIGN

The basic idea of our design is to make possible application of stress in a highly controllable way to the same sample undergoing multiple mounting-dismounting cycles between electron irradiation runs. Additional limitation is imposed by the fact that these mounting procedures cannot invoke soldering or any other heating, leading to sample annealing. For this reason contacts to the sample for four-probe resistivity measurements were permanently fixed and were also used to apply tensile stress similar to our previous design[11,12]. The novel elements introduced were (i) modification of the sample contact arrangement to make it easy to dismount; (ii) modification of the horseshoe device enabling simple sample mounting with silver paint; (iii) introduction of the strain gauge to enable stress monitoring.

The sample had four silver wire contacts permanently tin-soldered[13,14] (shown with black in Fig. 1), stable to electron

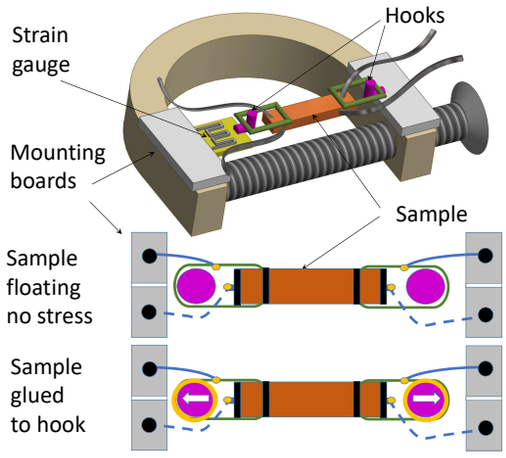

FIG. 1. (Color online) Schematics of the hook device developed for multiple stress applications to the same sample after mounting/dismounting cycles (top). Sample mounting (middle panel) for measurements in stress-free conditions. Sample contacts are glued with silver paint (orange) to supporting bent silver wires (blue lines) soldered (black dots) to the mounting boards. Sample is floating without touching hooks. For stress application (bottom panel) sample potential silver wires (green) are glued to hooks (magenta) with silver paint (orange). Big arrows indicate the direction of stress application.

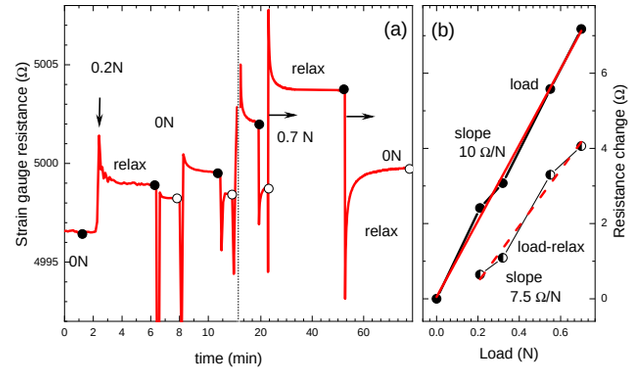

FIG. 2. (Color online) (a) Time dependence of the strain gauge resistance during loading (black solid dots) and relaxing (open circles) stress in the hook device. On application of force the strain gauge resistance shows transient (with relaxation tine gradually increasing with stress) and reaches stable value in several minutes (black solid dots). Relaxing force to zero does not bring the resistance completely back, with zero stress value gradually increasing (open circles). Note time scale break in (a). (b) Change of the strain gauge resistance as a function of force applied. Solid dots show change relative to the initial value before stress application, half filled circles show the difference between loaded and relaxed values [solid and open circles in panel (a)] for each force application step. The slopes of the curve determine stress sensitivity and its uncertainty.

irradiation[15]. Similar to our previous design[11], stress was applied through 50 μm silver wires forming potential contacts (green in Fig. 1). In the previous design these wires were directly soldered to the mounting boards at two hook arms. In the current design these stress-transmitting wires are glued with silver paint (orange in Fig. 1) to the hooks, formed by thick, 500 μm diameter silver wires (magenta in Fig. 1). Current wires on the sample were made short. The electrical contact to the sample was separated from the hook in stress-free conditions. Four silver wires (blue in the middle and bottom panels of Fig. 1) soldered to the mounting boards at two arms of the horseshoe device (gray) were bent to avoid stress and glued to four sample contacts with silver paint (orange dots in the middle and bottom panels of Fig. 1). This way sample properties can be measured in stress free conditions without attaching sample to the hooks.

One of the hooks was attached to a mounting board on a horseshoe device while the other was soldered to a thin plate of phosphorus bronze with strain gauge glued on top. The strain gauge was 5000 Ω FSM2-A6306S-500-SXEC gauge from *Vishay*.

In Fig. 2(a) we show response of the strain gauge resistance (SGR) to the force applied. Initially gauge resistance was slightly above 4996 Ω and stable in time. On application of stress resistance reached 5001 Ω and then relaxed to a stable value close to 4999 Ω. Releasing stress leads to a new transient with resistance undershooting the stable value, best seen for the relaxation of the highest stress of 0.7 N, where the relaxation time is the longest. Continuous (though small) increase of the strain gauge resistance limits our ability for precise stress determination. In addition in the configuration with connection of strain gauge to a wide plate there are unavoidable additional distortions in transverse direction. We evaluated the transverse strain as about 0.1 of the main stress by gluing strain gauge rotated by 90 degrees. As can be seen in Fig. 2(b) taking the difference of the strain gauge resistances with initial value (solid dots) gives a slope of 10 Ω/N, taking the difference to consecutive relaxed values (open circles in panel (a)) gives a slope of 7.5 Ω/N. So in the current design strain gauge is used as rather an indicator of stress level, not for precise stress measurement.

IV. ELECTRICAL RESISTIVITY MEASUREMENTS IN MECHANICAL DETWINNING DEVICE

We measured a single crystal of $Ba_{1-x}K_xFe_2As_2$ (x =0.25) which has two structural transitions: one is from tetragonal to orthorhombic phase at T_{C2} = 55 K and the other is re-entrant tetragonal transition at T_{C4} = 37 K. The sample was cut with the wire saw along tetragonal [110] direction in the plane. The sample dimensions were 3.2 ([110]-direction)×0.33([1-10] direction)× 0.11 ([001] direction) mm^3. The sample length between potential contacts was 1.64 mm.

In Fig. 3 we plot temperature-dependent electrical resistivity $\rho(T)$ (left panel) of the sample stretched using hook device with several levels of stress applied at room temperature. This stress value naturally varies on cooling, see right panel. The inset shows $\rho(T)$ of the sample over the whole range up to 300 K, with the resistivity value fixed at $\rho(300K)$ =300 $\mu\Omega cm$[20]. The right panel shows temperature dependence of

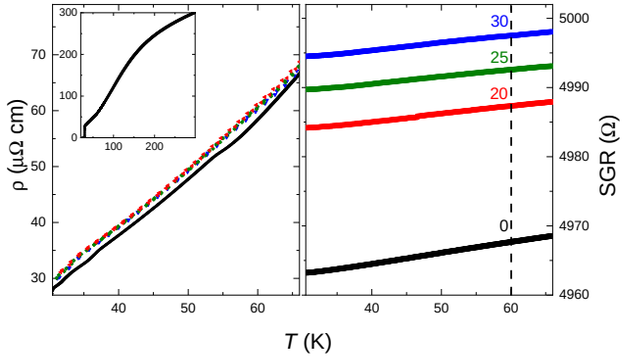

FIG. 3. Electrical resistivity of $Ba_{1-x}K_xFe_2As_2$ sample with x =0.25, zoomed in the range of tetragonal to orthorhombic phase transition (left panel). The curve colors correspond to those of the temperature-dependent strain gauge resistance (SGR) shown in the right panel. The black curve is measured in stress-free condition (ΔSGR=0) while the other curves measured under stress. The blue (ΔSGR=30 Ω) and green (ΔSGR=25 Ω) curves for higher stress levels almost perfectly coincide with red curve, and for this reason limited numbers of data points are shown. Actual data set for the red curve is shown below in Fig. 5. Inset of left panel shows the $\rho(T)$ dependence over the whole range to room temperature. Right panel presents temperature-dependent resistance of the strain gauge mechanically connected in series with the sample during the measurements. The increases of strain gauge resistance, ΔSGR at 60 K (dashed line), were used as stress measure in Fig. 4

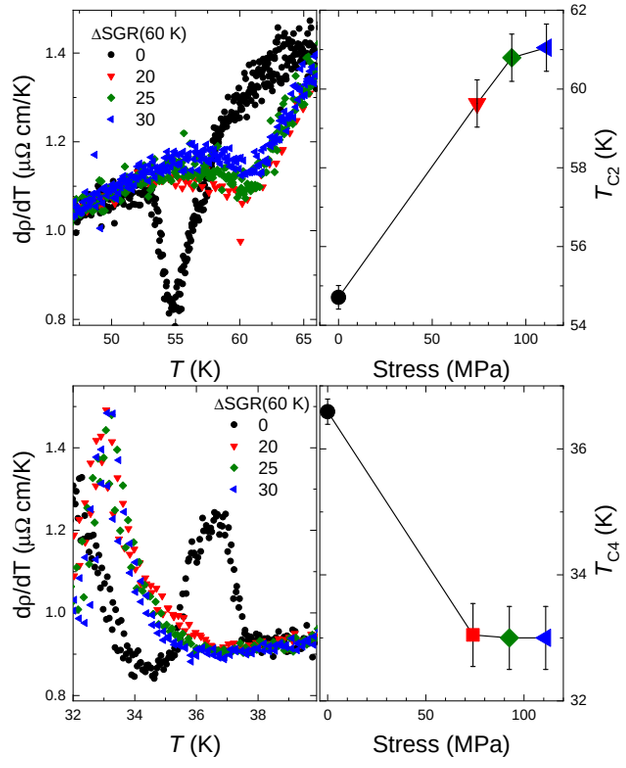

FIG. 4. Stress-evolution of the temperature dependent resistivity derivative, $d\rho/dT$, showing sharp features at tetragonal to orthorhombic C_2 transition (top panels) and C_4 transition (lower panels). Right panels show shifts of the transition temperatures with application of stress.

the strain gauge resistance, SGR, with numbers corresponding to SGR increase compared to stress-free state, ΔSGR. The strain gauge is mechanically connected in series with the sample and in ideal case experiences the same tensile force. The applied stress monotonically increases between runs.

The black curve was measured with sample floating on mounting silver wires over hook device in stress-free conditions. Measurements of the strain gauge resistance in this condition provides a baseline for its temperature dependence. Note that temperature variation of the gauge resistance is observed in stress-free conditions and the stress value is nearly temperature independent over the temperature range of particular interest, 30 to 80 K. Gluing sample wires to the hook creates stress in the series connected sample and the strain gauge as presented with red curves and changes notably temperature-dependent sample resistivity. Further increase of stress with push-screw provides notably smaller effect (green and blue curves). To make these changes visible we limit the number of the actual data points presented for each curve, otherwise they closely overlap. The difference in response is notable, however, close to small anomalies in $\rho(T)$ at the tetragonal to orthorhombic T_{C2} phase transition and the re-entrant tetragonal transition at T_{C4}.

The fact that the resistivity in the range between T_{C2} and T_{C4} does not evolve with the increase of stress suggests that the detwinning action of stress is complete. The sample is in the state with domains aligned by stress and the longer in-plane a-axis of the sample oriented along the tensile stress direction.

V. STRESS-DEPENDENCE OF STRUCTURAL TRANSITIONS

The temperature-dependent resistivity of the sample used in this study follows previous reports[15,17] with small upturn in $\rho(T)$ below 60 K signalling tetragonal-to-orthorhonbic phase transition at T_{C2} and small down-turn feature at 37 K signalling re-entrance of the tetragonal phase at T_{C4}[18–20]. These features in the $\rho(T)$ lead to clear anomalies in the temperature-dependent resistivity derivative, $d\rho(T)/dT$, see left panels of Fig. 4. Comparison with temperature-dependent resistivity under applied tensile stress clearly shows that in the vicinity of these features the response of the sample is the strongest. As can be seen by comparison of the temperature-dependent resistivity derivatives (Fig. 4) stress shifts the T_{C2} up and T_{C4} down, stabilizing orthorhombic phase with respect to the tetragonal phase.

The temperature independent shift of strain gauge resistance suggests that the tensile stress applied to the sample remains constant for each temperature sweep. The magnitude of the stress applied can be evaluated from change in strain gauge resistance, approximately 20 Ω for the first curve. Using the slope of the initial gauge resistance change line (10 Ω/N, Fig. 2(b)) this corresponds to a force of about 2 N, the slope for relaxed line (7.5 Ω/N, Fig. 2(b)) gives a value 2.7

N. For the sample of cross-section area of 3.6×10^{-8} m^2 this corresponds to a stress of 55 MPa and 74 MPa, respectively. These stress values are somewhat higher than usually used for detwinning, in 10 MPa range[21,23]. The stress dependence of T_{C2} and T_{C4} is shown in the right top and bottom panels of Fig. 4, respectively, using stress calibration with the slope for relaxed curve.

VI. IN-PLANE RESISTIVITY ANISOTROPY

The shifts of the phase transition temperatures under stress lead to sharp features in the plot of the difference between $\rho(74MPa) \equiv \rho_a$ and $\rho(0) \equiv \rho_t$ curves. This curve is closely linked with in-plane resistivity anisotropy[11,12]. Indeed due to multiple domain walls in the stress-free samples measured electrical resistivity ρ_t is equivalent mixture of ρ_a and ρ_b, $\rho_t = (\rho_a + \rho_b)/2$, thus $\rho_a - \rho_t = (\rho_a - \rho_b)/2$. In the right panel of Fig. 5 we show nematic resistivity ansiotropy $\rho_a - \rho_b = 2(\rho_t - \rho_a)$. Interestingly the sign of resistivity anisotropy in our sample is the same as reported[3] for slightly lower x, i.e. $\rho_a > \rho_b$, reversed compared to the electron-doped side[22]. Note that because of nearly zero stress sensitivity of the sample resistivity in the stress-detwinned state (compare curves for different stress values in the left panel of Fig. 3), the difference curve between T_{C2} and T_{C4} does not change with stress and is quite reproducible.

VII. ELECTRON IRRADIATION

After initial measurements in pristine conditions, the sample with contacts was removed from the detwinning device and mounted on a very thin (about 5 μm) mica plate in the hollow *Kyocera* chip. The chip was placed in the irradiation chamber and subjected to the flux of electrons of about 2.7 μA of electric current. This current was measured with the Faraday cage placed behind a hole in the sample stage, so that only transmitted electrons were counted. The accumulated irradiation dose is 2.35 C/cm^2. After irradiation the sample was re-mounted on the detwinning device and its temperature dependent resistivity was measured in a stress-free condition.

The irradiation increases resistivity of the sample by approximately 20 $\mu\Omega$cm, compare blue and green lines in the left panel of Fig. 5. It also suppresses notably T_{C4} in line with our previous results[15].

Gluing the sample to hook device created stress sufficient to detwin the sample (light green and cyan curves in the left panel of Fig. 5 , before and after irradiation, respectively). Stress-induced resistivity anisotropy[23,24] in the tetragonal phase above T_{C2} coincides with measurements before irradiation. The anisotropy in the orthorhombic phase increases notably, nearly doubling in magnitude. This result clearly shows that despite the anisotropy changes sign in the composition range $x \geq 0.20$ it is still linked with residual resistivity, similar to compositions on electron doped side.

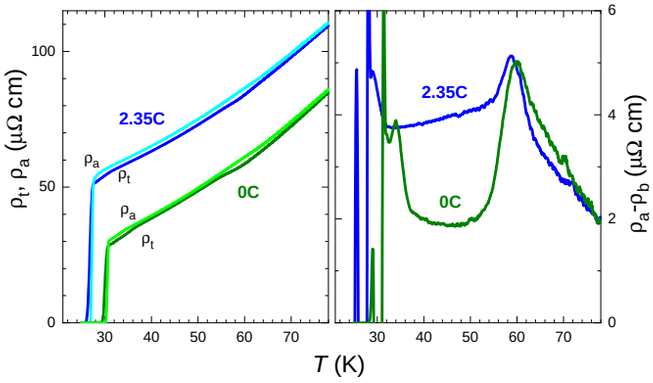

FIG. 5. Temperature-dependent resistivity of $Ba_{1-x}K_xFe_2As_2$ sample with x =0.25 in stress-free twinned state (dark green) and in stress-detwinned state achieved by application of uniaxial stress and measurements along a-axis in the orthorhomic plane. Blue and cyan curves show the resistivity in stress-free and strained conditions after electron irradiation with 2.35C/cm^2 dose. Right panel shows temperature-dependent nematic in-plane resistivity anisotropy, $\rho_a - \rho_b$. Note that sharp features at ∼35 K and ∼60 K are due to the shifts of T_{c2} and T_{c4} under stress. Green curve is for pristine sample, blue curve is for sample after electron irradiation. Note visible shift of T_{C4} down with irradiation.

VIII. SUMMARY

In summary, we developed a new design of stress-detwinning device enabling multiple sample mounting-dismounting cycles. The device performance is illustrated by studying stress-detwinning of hole doped $Ba_{1-x}K_xFe_2As_2$ sample with x =0.25 before and after electron irradiation with dose of 2.35 C/cm^2. We find stabilization of the C_2 phase under stress as would be naturally expected. The increase of residual resistivity as a result of electron irradiation is accompanied by the increase of in-plane resistivity anisotropy, arguing against the link between the low residual resistivity and the sign change of in-plane resistivity anisotropy.

ACKNOWLEDGMENTS

This research was supported by the U.S. Department of Energy, Office of Basic Energy Sciences, Division of Materials Sciences and Engineering. Ames Laboratory is operated for the U.S. Department of Energy by Iowa State University under Contract No. DE-AC02-0CH11358.

Irradiation realized on SIRIUS platform was supported by French National network of accelerators for irradiation and analysis of molecules and materials EMIRA under project 18-5354.

The data that support the findings of this study are available from the corresponding author upon reasonable request.

[1] S. Ishida, T. Liang, M. Nakajima, K. Kihou, C. H. Lee, A. Iyo, H. Eisaki, T. Kakeshita, T. Kida, M. Hagiwara, Y. Tomioka, T. Ito, and S. Uchida, "Manifestations of multiple-carrier charge transport in the magnetostructurally ordered phase of $BaFe_2As_2$," Phys. Rev. B **84**, 184514 (2011).

[2]E. C. Blomberg, M. A. Tanatar, A. Thaler, S. L. Bud'ko, P. C. Canfield, and R. Prozorov, "Multi-band effects in in-plane resistivity anisotropy of strain-detwinned disordered $Ba(Fe_{1-x}Ru_x)_2As_2$," J. Phys.: Condens. Matter **30**, 315601 (2018).

[3]E. C. Blomberg, M. A. Tanatar, R. M. Fernandes, I. I. Mazin, Bing Shen, Hai-Hu Wen, M. D. Johannes, J. Schmalian, and R. Prozorov, "Sign-reversal of the in-plane resistivity anisotropy in hole-doped iron pnictides," Nat. Commun. **4**, 1914 (2013).

[4]Maxim Breitkreiz, P. M. R. Brydon, and Carsten Timm, "Resistive anisotropy due to spin-fluctuation scattering in the nematic phase of iron pnictides," Phys. Rev. B **90**, 121104(R) (2014).

[5]A.C. Damask and G.J. Dienes, *Point Defects in Metals* (Gordon & Breach Science Publishers Ltd, London, 1963).

[6]K. Cho, M. Kończykowski, J. Murphy, H. Kim, M. A. Tanatar, W. E. Straszheim, B. Shen, H. H. Wen, and R. Prozorov, "Effects of electron irradiation on resistivity and London penetration depth of $Ba_{1-x}K_xFe_2As_2$ ($x \leq 0.34$) iron-pnictide superconductor," Phys. Rev. B **90**, 104514 (2014).

[7]Ruslan Prozorov, Marcin Kończykowski, Makariy A. Tanatar, Hai-Hu Wen, Rafael M. Fernandes, and Paul C. Canfield, "Interplay between superconductivity and itinerant magnetism in underdoped $Ba_{1-x}K_xFe_2As_2$ ($x = 0.20$) probed by the response to controlled point-like disorder," npj Quantum Mater. **4**, 34 (2019).

[8]Kyuil Cho, M. Kończykowski, S. Teknowijoyo, M. A. Tanatar, and R. Prozorov, "Using electron irradiation to probe iron-based superconductors," Supercond. Sci. Technol. **31**, 064002 (2018).

[9]I. R. Fisher, L. Degiorgi, and Z. X. Shen, "In-plane electronic anisotropy of underdoped '122' Fe-arsenide superconductors revealed by measurements of detwinned single crystals," Rep. Progr. Physics **74**, 124506 (2011).

[10]http://emir.in2p3.fr/, LSI, electron irradiation facility.

[11]M. A. Tanatar, E. C. Blomberg, A. Kreyssig, M. G. Kim, N. Ni, A. Thaler, S. L. Bud'ko, P. C. Canfield, A. I. Goldman, I. I. Mazin, and R. Prozorov, "Uniaxial-strain mechanical detwinning of $CaFe_2As_2$ and $BaFe_2As_2$ crystals: Optical and transport study," Phys. Rev. B **81**, 184508 (2010).

[12]E. C. Blomberg, M. A. Tanatar, A. Kreyssig, N. Ni, A. Thaler, Rongwei Hu, S. L. Bud'ko, P. C. Canfield, A. I. Goldman, and R. Prozorov, "In-plane anisotropy of electrical resistivity in strain-detwinned $SrFe_2As_2$," Phys. Rev. B **83**, 134505 (2011).

[13]M. A. Tanatar, N. Ni, S. L. Bud'ko, P. C. Canfield, and R. Prozorov, "Field-dependent transport critical current in single crystals of $Ba(Fe_{1-x}TM_x)_2As_2$ (TM = Co, Ni) superconductors," Supercond. Sci. Techn. **23**, 054002 (2010).

[14]M. A. Tanatar, R. Prozorov, N. Ni, S. L. Bud'ko, and P. C. Canfield, "Low resistivity contact to Iron Arsenide superconductors," U.S. Patent No. 8,450,246 (2011).

[15]E. I. Timmons, M. A. Tanatar, K. Willa, S. Teknowijoyo, Kyuil Cho, M. Kończykowski, O. Cavani, Yong Liu, T. A. Lograsso, U. Welp, and R. Prozorov, "Competition between orthorhombic and re-entrant tetragonal phases in underdoped $Ba_{1-x}K_xFe_2As_2$ probed by the response to controlled disorder," Phys. Rev. B **99**, 054518 (2019).

[16]Y. Liu, M. A. Tanatar, W. E. Straszheim, B. Jensen, K. W. Dennis, R. W. McCallum, V. G. Kogan, R. Prozorov, and T. A. Lograsso, "Comprehensive scenario for single-crystal growth and doping dependence of resistivity and anisotropic upper critical fields in $(Ba_{1-x}K_x)Fe_2As_2$ ($0.22 \leq x \leq 1$)," Phys. Rev. B **89**, 134504 (2014).

[17]E. Hassinger, G. Gredat, F. Valade, S. Renè de Cotret, A. Juneau-Fecteau, J.-Ph. Reid, H. Kim, M. A. Tanatar, R. Prozorov, B. Shen, H.-H. Wen, N. Doiron-Leyraud, and Louis Taillefer, "Pressure-induced Fermi-surface reconstruction in the iron-arsenide superconductor $Ba_{1-x}K_xFe_2As_2$: Evidence of a phase transition inside the antiferromagnetic phase," Phys. Rev. B **86**, 140502(R) (2012).

[18]A. E. Böhmer, F. Hardy, L. Wang, T. Wolf, P. Schweiss, and C. Meingast, "Superconductivity-induced re-entrance of the orthorhombic distortion in $Ba_{1-x}K_xFe_2As_2$," Nat. Commun. **6**, 7911 (2015).

[19]J. M. Allred, S. Avci, D. Y. Chung, H. Claus, D. D. Khalyavin, P. Manuel, K. M. Taddei, M. G. Kanatzidis, S. Rosenkranz, R. Osborn, and O. Chmaissem, "Tetragonal magnetic phase in $Ba_{1-x}K_xFe_2As_2$ from x-ray and neutron diffraction," Phys. Rev. B **92**, 094515 (2015).

[20]Yong Liu, M.A. Tanatar, E.I.Timmons, and T.A.Lograsso, "Polarized Light Microscopy Study on the Reentrant Phase Transition in a $(Ba_{1-x}K_x)Fe_2As_2$ Single Crystal with $x = 0.24$," Crystals, **6**, 142 (2016).

[21]T. Liang, M. Nakajima, K. Kihou, Y. Tomioka, T. Ito, C.H. Lee, H. Kito, A. Iyo, H. Eisaki, T. Kakeshita, S. Uchida, "Effects of uniaxial pressure and annealing on the resistivity of $Ba(Fe_{1x}Co_x)_2As_2$," J. Phys. Chem. Solids, **72**, 418 (2011).

[22]J-H. Chu, J.G. Analytis, K.D. Greve, P.L. McMahon, Z. Islam, Y. Yamamoto, and I.R. Fisher, "In-Plane Resistivity Anisotropy in an Underdoped Iron Arsenide Superconductor," Science **329**, 824 (2010).

[23]E. C. Blomberg, A. Kreyssig, M. A. Tanatar, R. M. Fernandes, M. G. Kim, A. Thaler, J. Schmalian, S. L. Bud'ko, P. C. Canfield, A. I. Goldman, and R. Prozorov, "Effect of tensile stress on the in-plane resistivity anisotropy in $BaFe_2As_2$," Phys. Rev. B **85**, 144509 (2012).

[24]M.A. Tanatar, A.E. Böhmer, E.I. Timmons, M. Schütt, G. Drachuck, V. Taufour, K. Kothapalli, A. Kreyssig, S.L. Bud'ko, P.C. Canfield, R.M. Fernandes, and R. Prozorov, "Origin of the Resistivity Anisotropy in the Nematic Phase of FeSe," Phys. Rev. Lett. **117**, 127001 (2016).

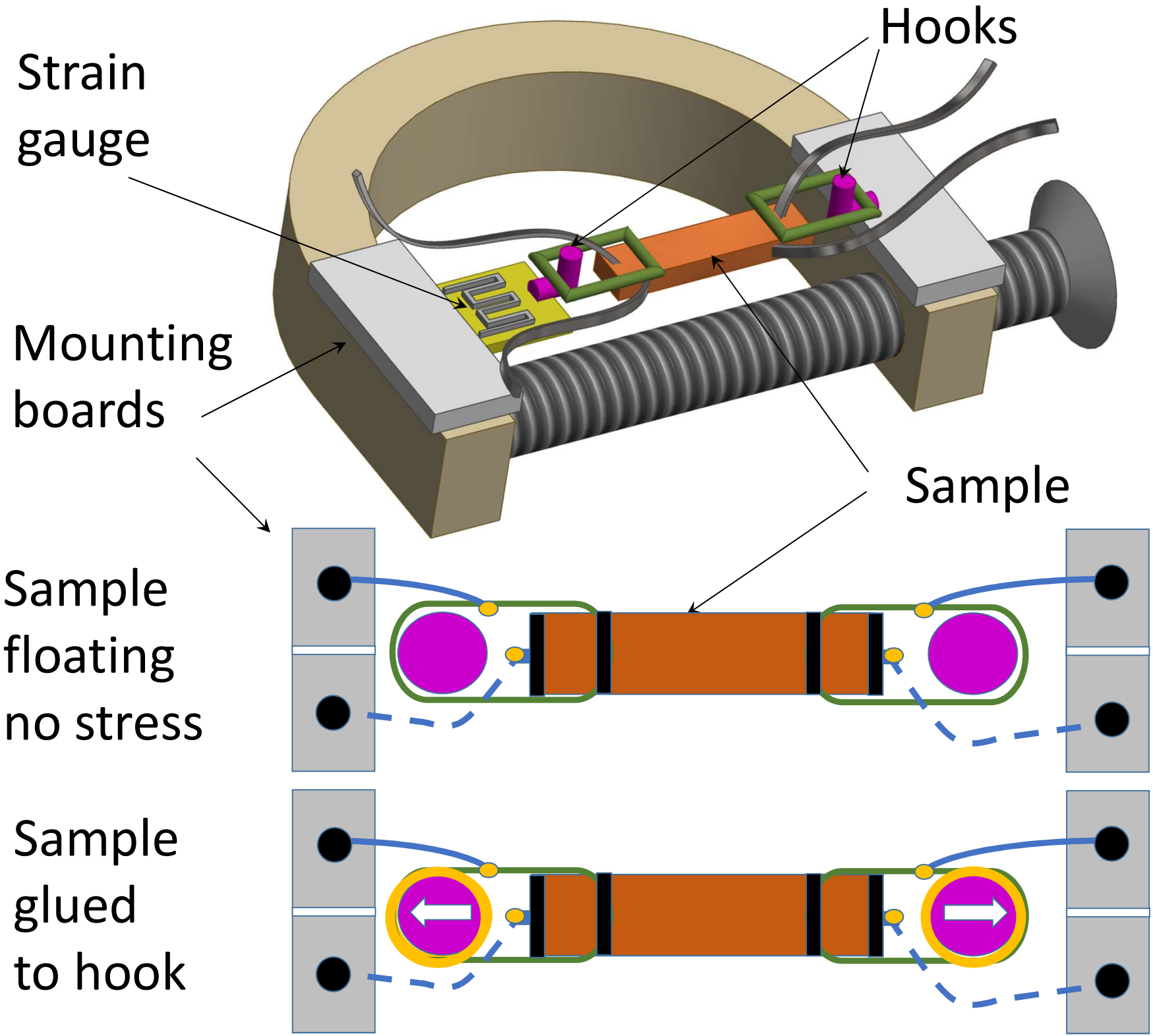
Strain gauge
Hooks
Mounting boards
Sample
Sample floating no stress
Sample glued to hook

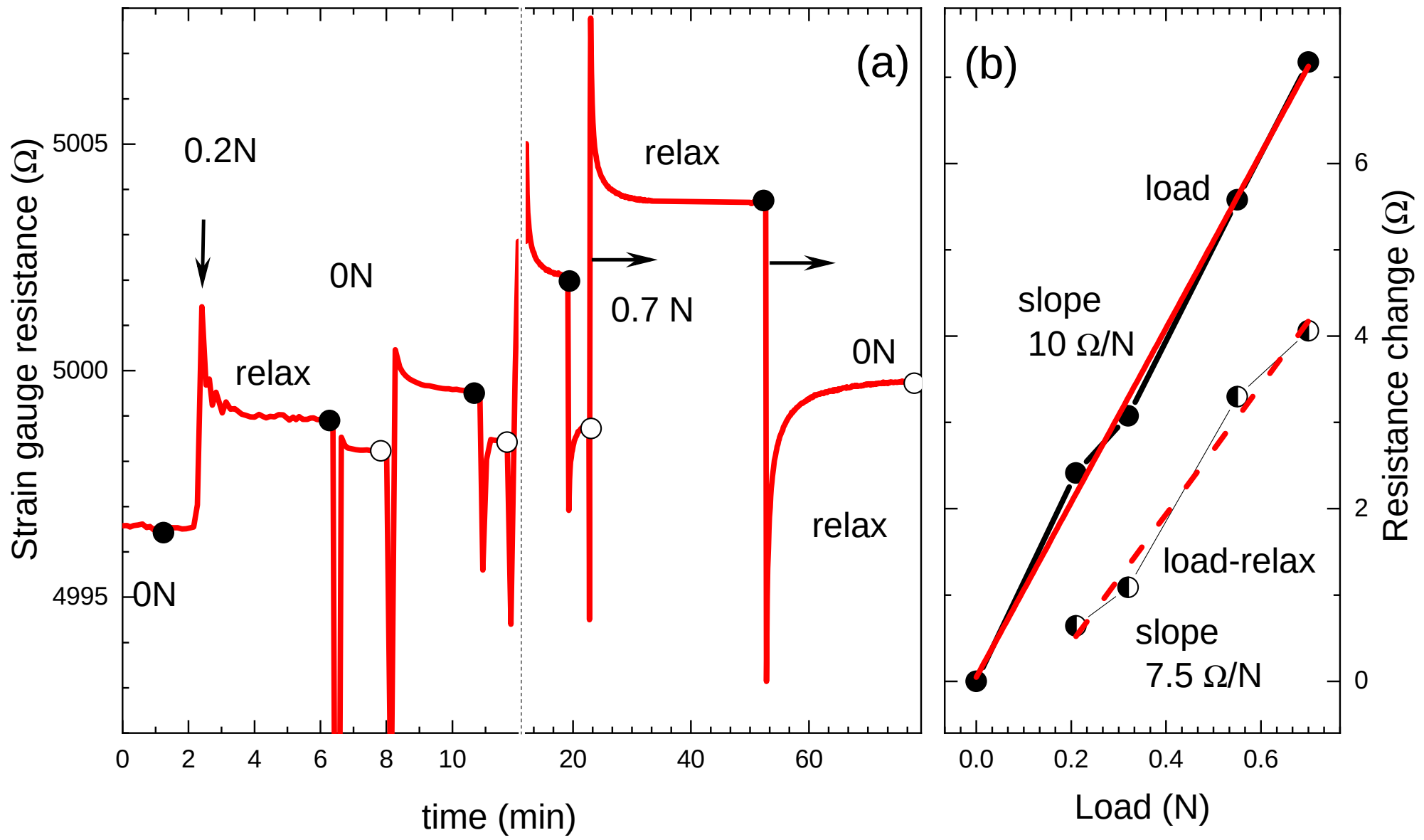
(a)
(b)
0.2N
0N
relax
0.7 N
relax
0N
relax
0N
Strain gauge resistance (Ω)
5005
5000
4995
0
2
4
6
8
10
20
40
60
time (min)
load
slope
10 Ω/N
load-relax
slope
7.5 Ω/N
Resistance change (Ω)
0
2
4
6
0.0
0.2
0.4
0.6
Load (N)

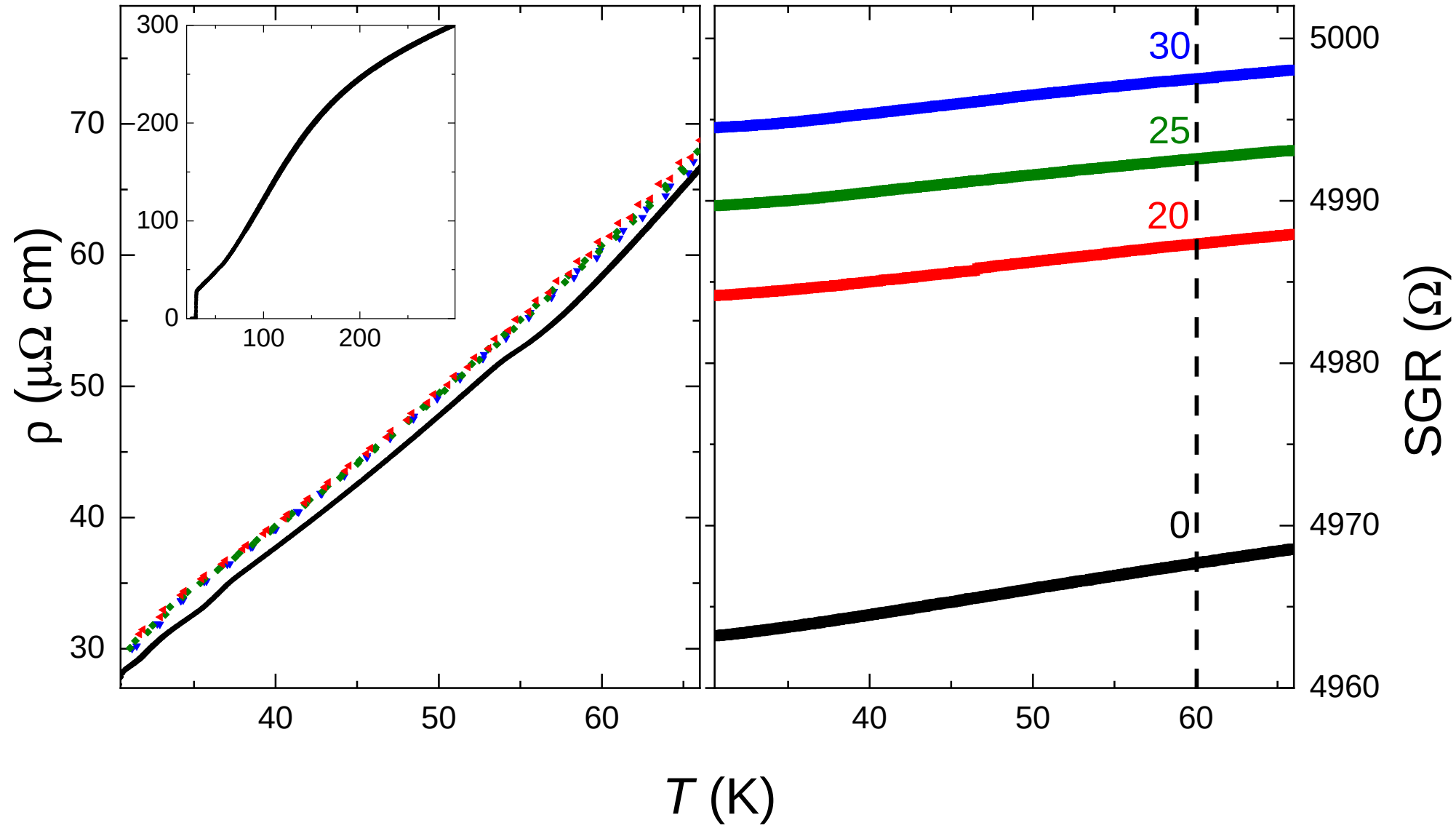
ρ (μΩ cm)
70
60
50
40
30
40
50
60
300
200
100
0
100
200
30
25
20
0
5000
4990
4980
4970
4960
SGR (Ω)
T (K)

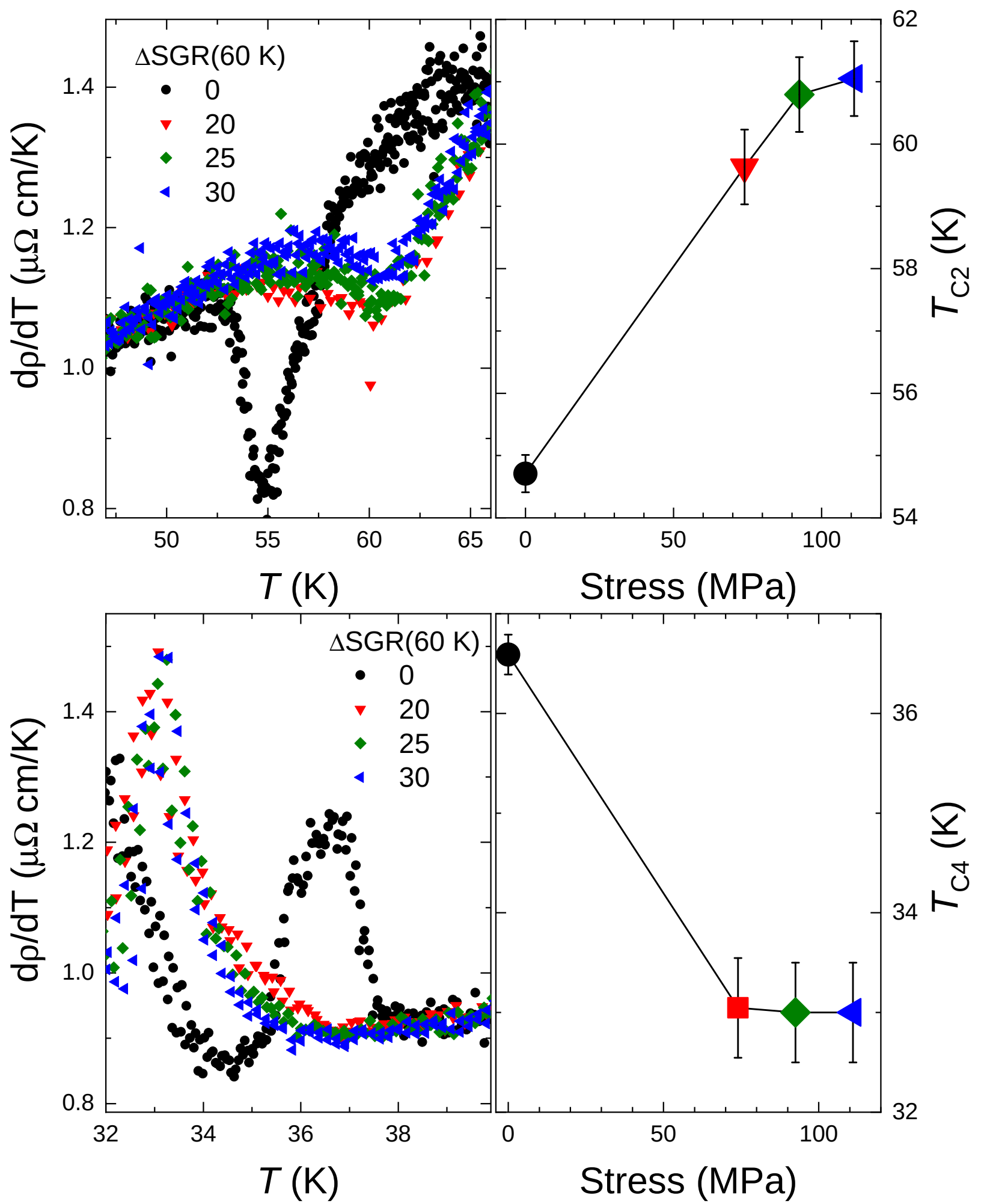
ΔSGR(60 K)
0
20
25
30
dρ/dT (μΩ cm/K)
T (K)
Stress (MPa)
T_C2 (K)
T_C4 (K)

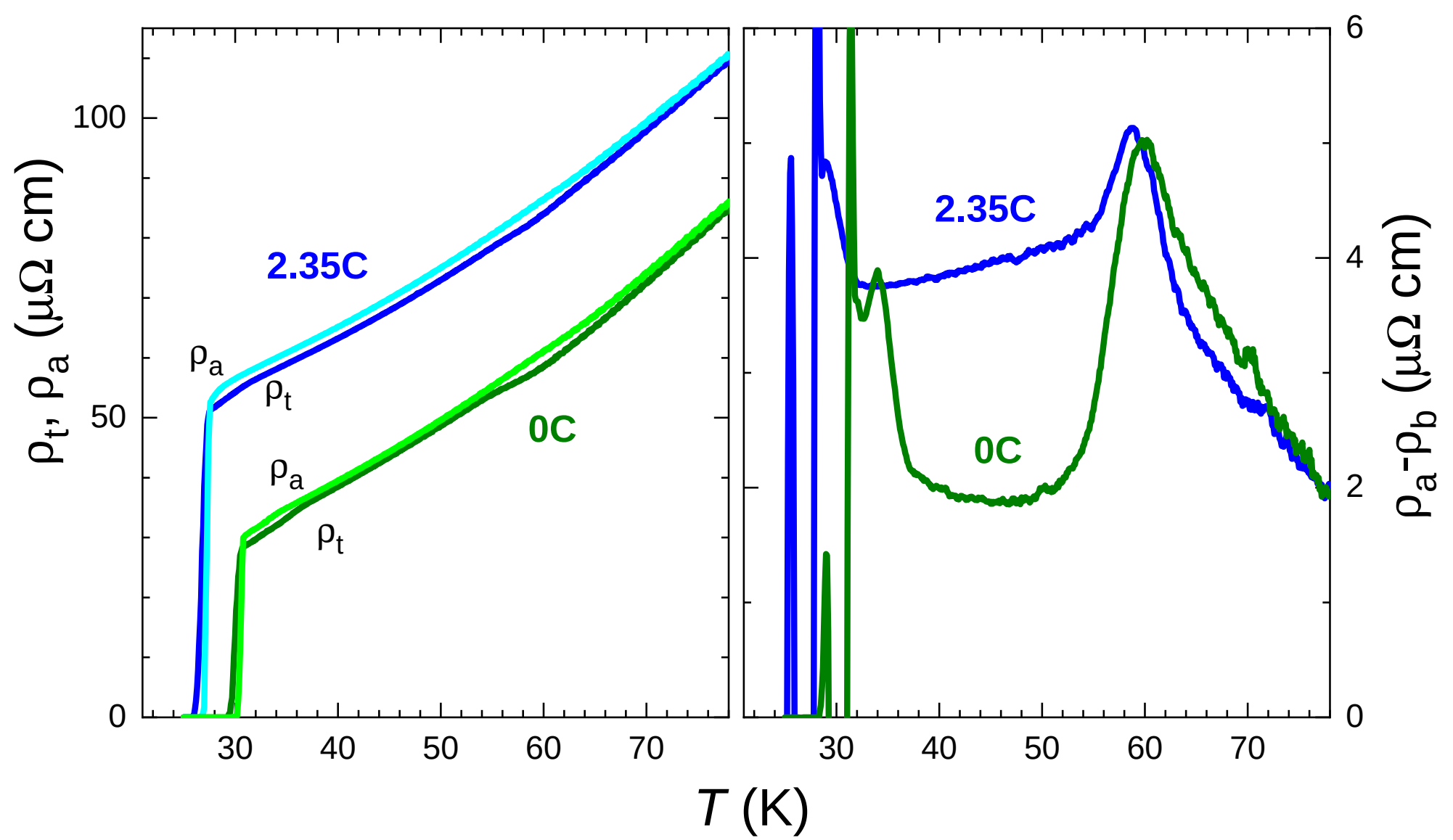
100
50
0
30
40
50
60
70
ρ_t, ρ_a ($\mu\Omega$ cm)
2.35C
ρ_a
ρ_t
0C
ρ_a
ρ_t
2.35C
0C
6
4
2
0
ρ_a-ρ_b ($\mu\Omega$ cm)
T (K)